Energy Expenditure during Cell Spreading Induces AMPK Activation and Regulates the Mechanoresponse of Stem Cells

Jing Xie [1,†], Min Bao [1,†], Xinyu Hu [1], Werner J. H. Koopman [2], Wilhelm T. S. Huck [1,]*

[1] Institute for Molecules and Materials, Radboud University, Heyendaalseweg 135, 6525 AJ Nijmegen, The Netherlands.

[2] Department of Biochemistry, Radboud Institute for Molecular Life Sciences, Radboud University Medical Centre, Geert Grooteplein 28, 6525 GA, Nijmegen, The Netherlands.

[*] Corresponding author. Email: w.huck@science.ru.nl

[†] These authors contributed equally to this work

Abstract

Cells respond to the mechanical properties of the extracellular matrix (ECM) through formation of focal adhesions (FAs), re-organization of the actin cytoskeleton and adjustment of cell contractility. These are energy-demanding processes, but a potential causality between mechanical cues and cellular (energy) metabolism remains largely unexplored. Here, we demonstrate that cytoskeletal reorganization and FA formation during cell spreading on stiff substrates lead to a drop in intracellular ATP levels, thereby activating AMP-activated protein kinase (AMPK). The latter then triggers rapid mitochondrial fragmentation and an increase in ATP levels to reinforce cell tension and regulate nuclear localization of YAP/TAZ and Runx2. Genetic ablation of AMPK Thr-172 phosphorylation lowered cellular ATP content and strongly reduced responses to substrate stiffness. Together, these findings reveal the importance of energy expenditure in regulating the mechanoresponse of cells, and point to AMPK as a key mediator of stem cell fate in response to ECM mechanics.

1. Introduction

The physical properties of the extracellular matrix (ECM) have a profound impact on cell behavior and stem cell fate, and a direct relationship between matrix stiffness, cell spreading and lineage selection has been demonstrated [1-6]. Forces generated within the actin cytoskeleton and transmitted through FAs, play a major role in the cellular response to biophysical cues [7-10]. Much attention has been given to how cells respond to mechanical forces. However, less is known how these forces are integrated with other cellular processes including bioenergetics [11-13]. In order to understand how mechanical forces shape the cellular phenotype and regulate cell fate, it is necessary to consider the highly dynamic nature of the cellular response, which involves a hitherto overlooked large energy expenditure. Growing evidence indicates that the transduction

of external mechanical forces are linked to metabolic signals such as neutral lipid synthesis [13], mitochondrial structural remodeling [14], cellular glucose uptake [11] and cell migration [15]. The cellular response is a well-tuned process that must balance energy supply with energy demand to allow proper actin polymerization, FA formation and cellular contractility buildup. But it remains unclear how cells respond to this energy expenditure, tune energy supply and demand, and maintain energy homeostasis for mechanotransduction.

AMPK, a well-characterized cellular energy sensor [15, 16], plays a key role in the coordination of cell function by controlling intracellular ATP levels [17]. AMPK is Thr172-phosphorylated and thereby activated (yielding pAMPK) when the AMP/ATP ratio increases, for instance during starvation, hypoxia or cell detachment from the ECM [18, 19]. Upon AMPK activation, energy homeostasis is restored by altering mitochondrial morphology or glucose, protein and lipid metabolism [20]. AMPK is a key regulator of mitochondrial dynamics, as it can phosphorylate and thereby activate a mitochondrial fission factor (Mff), which stimulates mitochondrial division [21, 22]. Alterations in mitochondrial fission, fusion and morphology are induced by mechanical cues, chemical stimulations or metabolic stresses [22-24]. A recent study in MCF10A (human breast epithelial) cells and MDCK II (canine kidney epithelial) cells, revealed that force-mediated AMPK activation stimulated actomyosin contractility and increased cellular ATP levels, thus linking energy homeostasis with cell-cell adhesion mechanotransduction [11]. Actomyosin contractility also plays a major role in the cellular response to the physical properties of the ECM through FA formation and organization of the actin cytoskeleton, which are ATP-dependent [11, 12, 25, 26]. We hypothesized that the very expenditure of ATP during spreading regulates the cellular mechanoresponse to physical cues.

In this study, we demonstrate how the AMPK energy sensor is activated by the spreading-induced drop in cellular ATP levels to restore the energy homeostasis via altering mitochondrial morphodynamics. On a stiff substrate, we observed high ATP levels, increased glucose uptake and actomyosin contractility, and continuous AMPK activation, resulting in nuclear localization of YAP/TAZ and Runx2, and osteogenic differentiation. Cell fate appeared strongly correlated with the activation or inhibition of AMPK, independent of substrate stiffness. Our findings establish a critical role for AMPK in connecting intracellular energy expenditure and cellular mechanotransduction, with downstream effects on stem cell fate.

2. Results

2.1 Feedback between spreading and intracellular energy expenditure

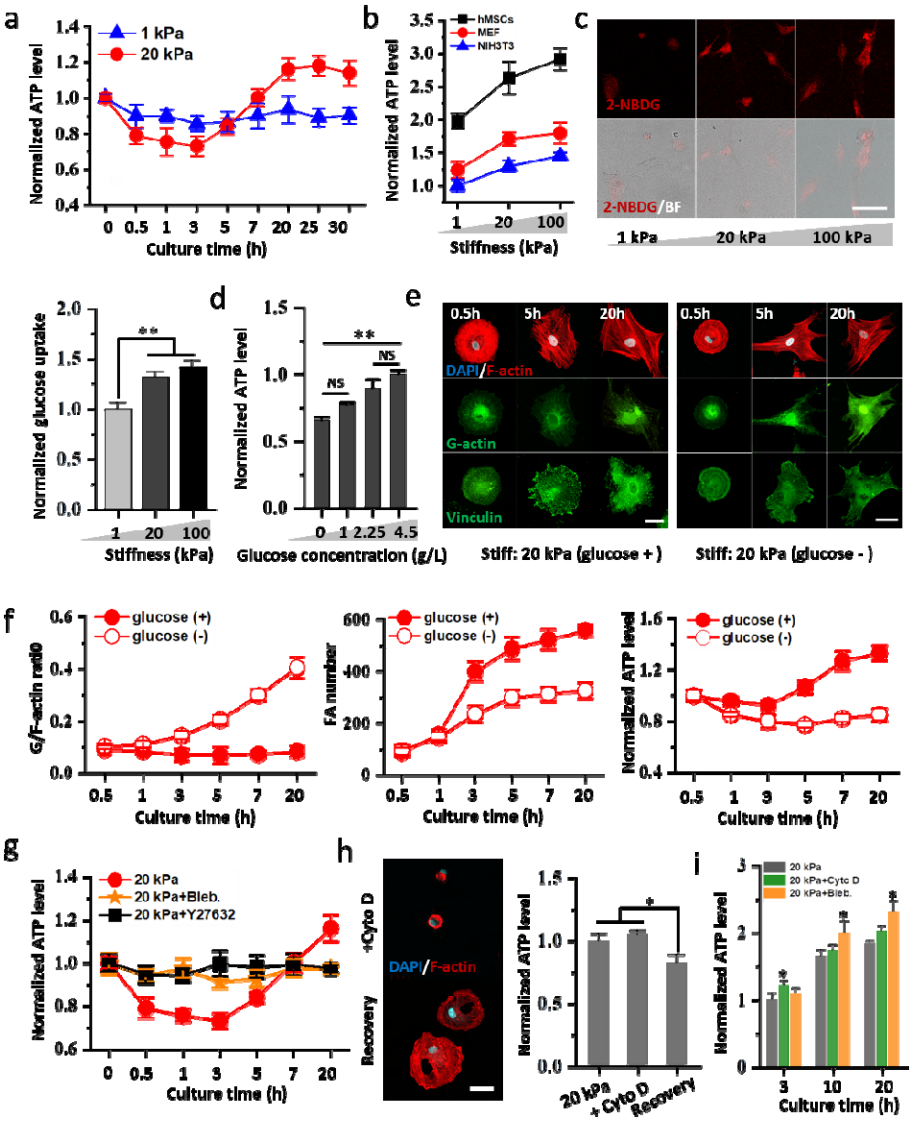

Fig. 1 Organization of actin cytoskeleton and FA formation correlates with intracellular ATP levels. (A) Normalized ATP level of hMSCs cultured on soft (1 kPa) and stiff (20 kPa) PAAm gels over time (n=6). (B) ATP levels in different kinds of cells (hMSCs, MEF, NIH3T3) cultured on PAAm gels at 20 h after seeding with variable stiffness (1, 20 and 100 kPa) (n=6). (C) Glucose uptake on different substrate visualized by 2-NBDG (red). Graph: quantification of 2-NBDG intensity (n=5, N=3). Scale bars, 100 µm. (D) ATP intensities of hMSCs over 20 h culturing on stiff PAAm gels with different glucose concentration (n=6, N=3). (E) Confocal images of hMSCs cultured in the presence (left) or absence of glucose (right) on stiff PAAm gel showing G-actin (DNaseI-labeled staining: green) and FAs (vinculin staining: green) at different time points. F-actin was stained with phalloidin (red) and nuclei were counterstained with DAPI (blue). Scale bars, 50 µm. (F) Quantification of G/F actin ratio (n>25 representative cells, N=3), FA number (n>25 representative cells, N=3) and normalized ATP levels (n=6) in hMSCs cultured under glucose starvation on stiff PAAm gel. (G) Normalized ATP intensity in hMSCs cultured on stiff PAAm gel treated with 50 µM myosin inhibitor Blebbistatin (Bleb.) or 50 µM Rock inhibitor Y27632 (n=6). (H) Actin disassembly with 2.5 µM Cytochalasin D (Cyto D) and actin recovery after removal of Cyto D. Confocal images showed the changes in cellular morphologies. Graph shows changes in intracellular ATP intensity (n=6).

Scale bars, 50 µm. (I) Quantification of intracellular ATP intensity after 1 h of treatment with Cyto D and Bleb. at 3, 10 and 20 h after seeding (n=6).

We cultured human mesenchymal stem cells (hMSCs) (at low densities, 1250 cells/cm^2) on 1 kPa (soft) or 20 kPa (stiff) polyacrylamide (PAAm) gels functionalized with collagen (50 µg/mL), and determined intracellular ATP levels at different time points, from initial adhesion and spreading of cells to steady state (when no further morphological changes were observed) (**Fig. 1a and Supplementary Fig. 1a, b**). Consistent with previous findings [1, 5], cells grown on stiff substrates displayed larger cell spreading areas with reinforced stress fibers and accompanying lower levels of G-actin, and greater sizes and numbers of FAs (**Supplementary Fig. 1c-d**). During the same time window, intracellular ATP levels on the stiff substrate decreased by ~27% within the first 3 h (**Fig. 1a**), consistent with increased energy expenditure for spreading cells and concomitant formation of actin cytoskeleton and FAs. At steady state (no further changes in spread area after 20 h), intracellular ATP levels on stiff substrates recovered and even exceeded those on soft ones (**Fig. 1a**). Mouse embryonic fibroblasts (MEF) and NIH 3T3 cells also displayed increased intracellular ATP levels when cultured for 20 h on substrates of increasing stiffness (**Fig. 1b)**. A 31% increase in glucose uptake in hMSCs cultured on 20 kPa compared to 1 kPa PAAm substrates was determined from the higher intracellular levels of 2-NBDG, a fluorescent glucose analog used for monitoring glucose uptake into living cells (**Fig. 1c)**. A correlation between energy demand and spreading was also evident in glucose starvation experiments. Reducing glucose concentration in culture medium from 4.5 to 0 g/L for cells on stiff substrates significantly impacted on intracellular ATP levels (~34% lower; **Fig. 1d**) and starvation halted cell proliferation (**Supplementary Fig. 2**). To investigate the role of glucose in more detail, we monitored hMSC spreading on stiff substrates in the presence or absence of glucose **(Fig. 1e and Supplementary Fig. 1b, 3)**. Glucose depletion significantly reduced actin polymerization and FA formation, corroborated by 3.8-fold increase in G/F-actin levels (**Fig. 1f**) after 20 h culture. Cells cultured on stiff substrates in the presence of ROCK inhibitor Y27632 or myosin inhibitor blebbistatin (Bleb.) showed stable cellular ATP levels consistent with a less developed actin cytoskeleton and reduced cell contractility (**Fig. 1g and Supplementary Fig. 4**). Next, we studied the temporal characteristics of intracellular ATP changes upon disruption and re-organization of the actin cytoskeleton. Cells were treated for 1 h with Cytochalasin D (CytoD), after which they displayed a small rounded morphology and slightly increased ATP levels. After CytoD removal from the medium, cells re-spread on the substrate, during which intracellular

ATP levels dropped by ~22% (**Fig. 1h**), confirming that actin cytoskeleton organization indeed consumes a significant fraction of intracellular ATP. Extending the CytoD treatment time to 5 h resulted in lower steady state ATP levels ~16% lower) and limited cell spreading (**Supplementary Fig. 5**).

Finally, we studied the contribution of cytoskeletal reorganization and cell tension buildup to ATP consumption on stiff substrates, by inhibiting actin polymerization and cytoskeletal tension using CytoD and Bleb., respectively, at different time points (**Fig. 1i**). For ease of comparison, ATP intensities were normalized to the non-treated control group at the particular time point. At early time points (< 5 h), inhibition by CytoD restored intracellular ATP levels (up 1.2 fold - back to levels of spreading cells); whereas Bleb. treatment had no significant effect. In contrast, at later time points (10 h and 20 h), treatment with CytoD did not lead to increases in ATP levels, but the addition of Bleb. Did, showing a 12 % increase. These results indicate that during early stages of cell spreading, ATP expenditure is mostly due to actin polymerization, whereas at steady state, increased cell contractility is a major route for ATP consumption.

2.2 Energy regulation through AMPK-mediated mitochondrial morphodynamics

In stem cells, mitochondria are prime generators of ATP [14, 22], these organelles are motile, and continuously fuse and divide, a process influenced by mechanical cues [14, 23]. In addition to its role in ATP production, mitochondrial dynamics has been coupled to the coordination of self-renewal vs. differentiation of stem cells [27]. Primed by these findings we next determined whether substrate stiffness affected mitochondrial morphology and dynamics. Visual inspection suggested that, on soft substrates, mitochondria display a filamentous structure at both 5 h and 20 h after seeding. In contrast, mitochondrial morphology appeared more fragmented on stiff substrates (**Fig. 2a**). Quantitative analysis [28] revealed that the mitochondria area (*Am*, a measure of mitochondrial size) and form factor (*F*, a combined measure of mitochondrial length and degree of branching), were significantly higher on soft than on stiff substrates (**Fig. 2b, c**). Functionally, the mitochondrial accumulation of the fluorescent cation tetramethylrhodamine methyl ester (TMRM) was higher in cells on stiff substrates (**Supplementary Fig. 6**). This suggests that the mitochondrial membrane potential, which provides a large part of the driving force for mitochondrial ATP production, is more negative [28]. Finally, time-lapse imaging of mitochondria revealed fast mitochondrial fission on stiff substrates, suggesting faster

mitochondrial dynamics (**Fig. 2d** and **Supplementary Movie**). Western blot analysis revealed increased pAMPK/AMPK ratios in hMSCs cultured for 5 and 20 h on stiff *vs.* soft substrates (**Fig. 2e**). To gain insight into the chain of events during AMPK phosphorylation we performed western blot and immunostaining analysis at different time points (**Fig. 2f, g**). On stiff substrates, virtually no pAMPK expression was observed during the initial cellular adhesion period (0.5 h) **(Fig. 2f).** Cells cultured on these substrates for longer than 1 h showed elevated pAMPK levels as well as nuclear localization. Together, these experiments establish that AMPK phosphorylation is preceded by a drop in ATP levels (**Fig. 1a** and **Fig. 2f, g**). Consistent with AMPK-mediated Mff activation, a fragmented mitochondrial phenotype was observed 1 h after seeding (**Supplementary Fig. 7**).

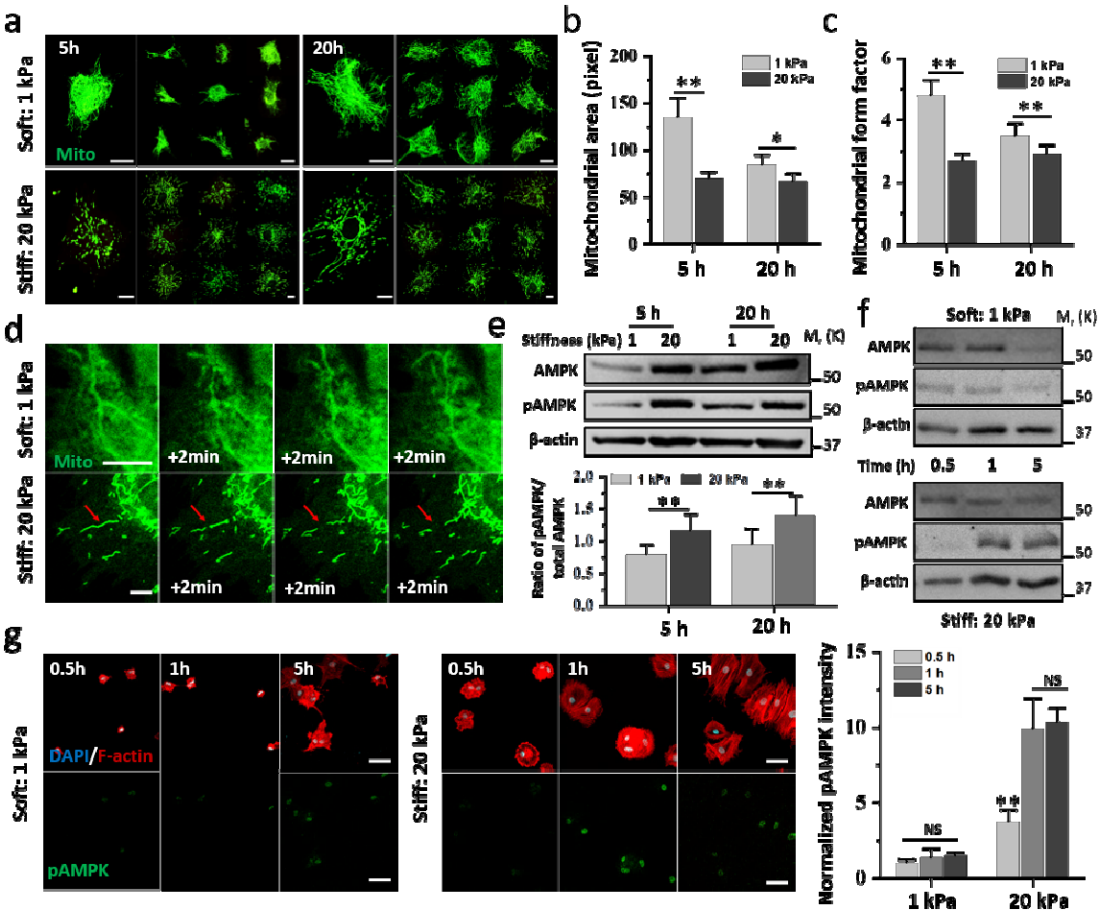

Fig. 2 Changes in mitochondrial dynamics mediated by AMPK correlate with ECM mechanics. (A) Mitochondrial morphologies on soft or stiff PAAm gels at 5 or 20 hours after seeding. Mitochondria were stained with Mito tracker (green). Scale bars, 25µm. (B, C) Quantification of (B) mitochondrial area and (C) form factor of the cells shown in (b) (n>25 representative cells from three independent experiments). (D) Time-lapse images of hMSCs cultured on PAAm gels of different stiffness stained with Mito tracker. Red arrows point to fast mitochondrial fission on stiff substrates. Scale bars, 10 µm. (E) Western blots of AMPK and Thr172-phosphorylated

AMPK (pAMPK) after 5 or 20 h incubation on different PAAm gels. Graph: quantification of the ratio of pAMPK to total AMPK. (F) Western blots of AMPK and pAMPK of cells at different time points after seeding. (G) Confocal images of hMSCs stained with antibodies against pAMPK (green) and counterstained with DAPI (blue) and actin (red) at different time points after seeding. Scale bars, 50 µm. Graph: quantification of pAMPK fluorescence intensity in single cells cultured on different PAAm gels at different time points (n>10 representative images).

2.3 Mechanotransduction is AMPK-dependent

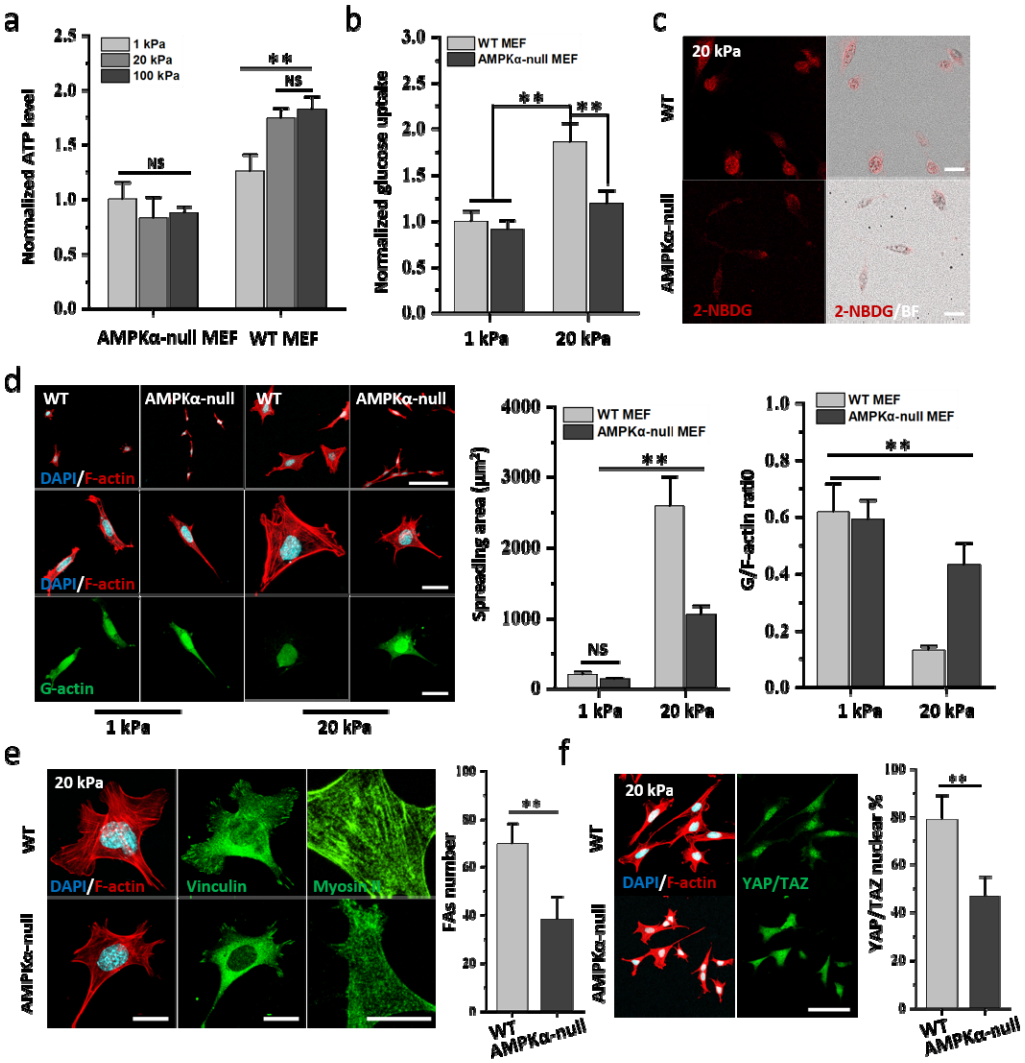

Fig. 3 AMPK-mediated energy metabolism drives mechanotransduction, independent of stiffness. (A) Normalized ATP levels in WT-MEF and AMPKα-null MEF cultured on 1, 20 and 100 kPa PAAm gels at 20 h after seeding (n=6). (B) Quantification of glucose taken up on different substrate (n=5, N=3). (C) Confocal images showing 2-NBDG (red) uptake on stiff substrate. Scale bars, 100 µm. (D) WT-MEF and AMPKα-null MEF cultured on stiff substrate demonstrating F-actin (red) and G-actin (green) after 20 h culture. Top: scale bar 100 µm; middle: scale bar 25 µm; bottom: scale bar 25 µm. Graph: quantification of spreading area (n>80 representative cells, N=3), and G/F-actin ratio (n>25 representative cells, N=3). (E) Vinculin (middle: green) and Myosin II (right: green) expression in cells cultured on stiff substrate. Scale bar 25, µm. Graph: quantification of FA numbers (n>25 representative cells, N=3) in cells cultured on stiff substrate. (F) YAP/TAZ localization in WT and AMPKα-null cells on stiff substrates. Cells were stained with YAP/TAZ (green), F-actin and nuclei were counterstained with phalloidin (red) and DAPI (blue). Scale bars, 100 µm. Graph: Quantification of YAP/TAZ nuclear localization (n>40 representative cells, N=3) in single cells on stiff substrate.

To establish the key role of AMPK in mechanotransduction, we cultured *AMPKα1*$^{-/-}$ *AMPKα2*$^{-/-}$ (AMPK*α*-null) mouse embryonic fibroblasts (MEFs) on soft and stiff substrates. These cells displayed a 40-50% lower ATP content that was not affected by stiffness **(Fig. 3a)**. Also, no differences in glucose uptake were observed for AMPK*α*-null MEFs cultured on different substrates **(Fig. 3b)**, which is lower compared to wild type (WT) MEFs on either substrate **(Fig. 3b, c)**. Interestingly, cell morphology of WT and AMPK*α*-null cells and on soft substrates appeared very similar **(Fig. 3d)**, but on stiff substrates AMPK*α*-null cells displayed limited spreading, and a less well-developed actin cytoskeleton (as evidenced by the ~2.3-fold higher G/F-actin ratio). **Fig. 3e** demonstrates reduced actomyosin contractility in AMPK*α*-null cells on stiff substrates and a lower number of FAs. YAP/TAZ is a mechanical regulator that typically shows cytoplasmic or nuclear localization regulated by external signals. [29, 30]. Stiff substrates and actomyosin tension are associated with high levels of nuclear YAP/TAZ [3, 31], and in WT cells we observed nuclear localization in up to 79±10% cells. Conversely, inhibition of actin polymerization and stress fiber formation by silencing AMPK almost halved YAP/TAZ nuclear localization **(Fig. 3f)**.

2.4 AMPK inhibition-induced ATP reduction limited cellular mechanotransduction

To further dissect the role of AMPK, we inhibited its phosphorylation with the cell-permeable inhibitor Compound C. 30 min after hMSCs seeding on stiff PAAm gels, AMPK inhibitor was added to medium for the following 20 h incubation which resulted in markedly decreased intracellular ATP levels (**Fig. 4a**). Compound C reduced glucose uptake by ~13% (**Fig. 4b**) and induced a shift in mitochondrial morphology from a fragmented to a more filamentous phenotype (**Fig. 4c**). The latter is comparable to the morphology changes induced by stiff (fragmented) and less stiff (filamentous) substrates (**Fig. 4c**). AMPK plays a dual role in migrating cells, stimulating cytoskeletal dynamics in the leading edge of lamellipodia, but inhibiting integrin activity and mechanotransduction in the more mature lamellum region [12]. Inhibition of AMPK clearly influenced FAs, which appeared smaller and confined to the edge of spreading cells (**Fig. 4d**). Furthermore, cytoskeletal organization was less developed, with fewer cross-cell stress fibers. Although cells displayed a similar spreading area, the number of FAs in cells decreased with increasing concentrations of Compound C. YAP/TAZ was increasingly localized in the cytoplasm with declining ATP levels after inhibition of AMPK (**Fig. 4e, f**).

Furthermore, we modulated energy supply by varying the glucose concentration in the culture medium. YAP/TAZ nuclear localization only became pronounced at glucose concentrations >2.5 g/L and during glucose starvation YAP/TAZ nuclear localization was as low as ~21±9% (**Supplementary Fig. 8**). Nuclear YAP/TAZ localization induced by ECM stiffness requires RhoA activity, which can regulate the formation of actin bundles, stress fibers and tensile actomyosin structure [32]. With the inhibition of AMPK, RhoA expression also decreased contributing to cytoplasmic YAP/TAZ localization. Interestingly, AMPK inhibition lead to lower levels of myosin II and β-integrin, suggesting a direct role for AMPK in regulating cell contractility [33] (**Fig. 4g**). Finally, cell proliferation after 48 h culture was completely suppressed upon Compound C addition (**Fig. 4h**). These results support the hypothesis that energy metabolism and mechanotransduction are linked.

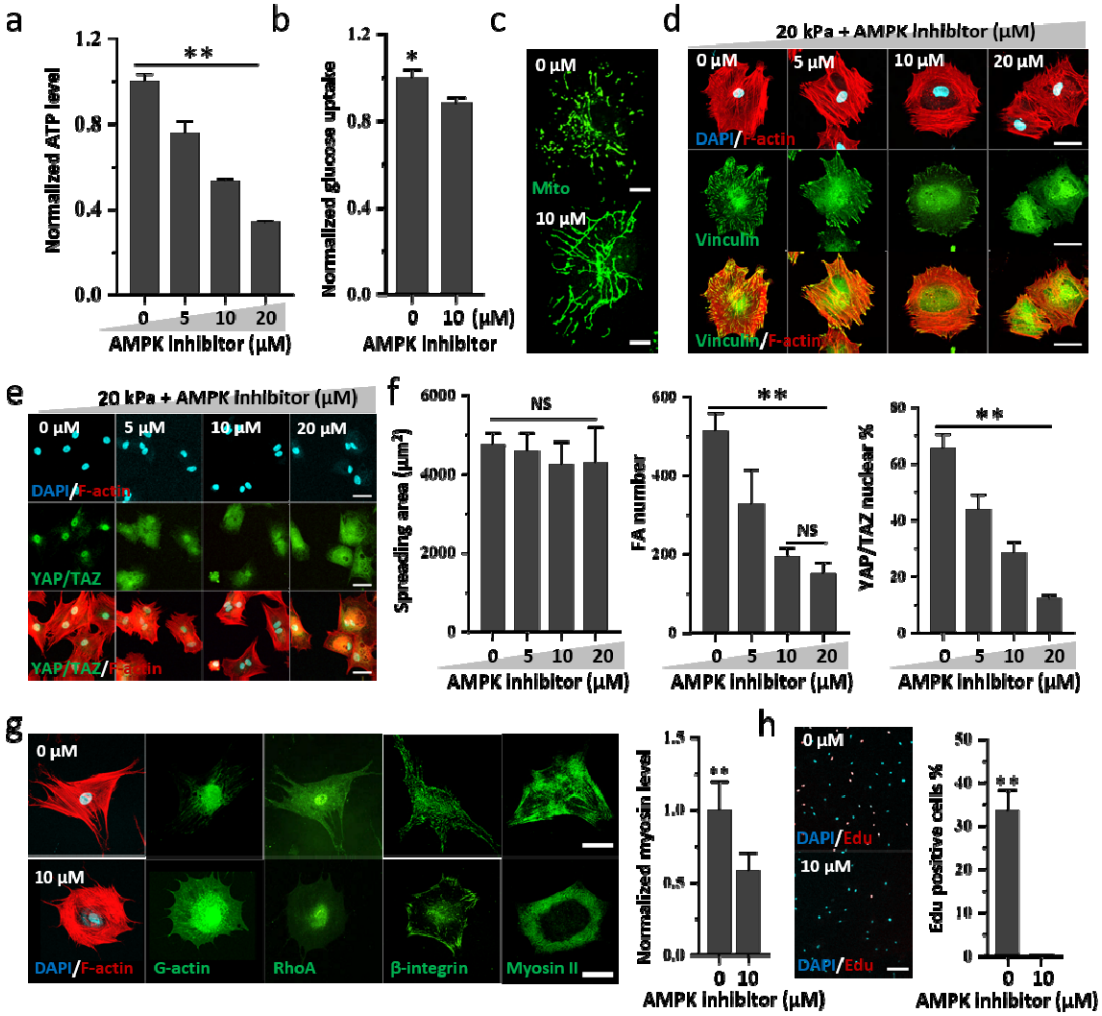

Fig. 4 AMPK inhibition is sufficient to regulate cellular response. (A) ATP levels and (B) glucose uptake in cells treated with variable concentrations of AMPK inhibitor (Compound C) on stiff substrate (n=5, N=3). (C)

Comparison of mitochondrial morphologies on stiff substrates with (bottom) or without (top) AMPK inhibitor treatment. Scale bars, 20 µm. (D, E) Confocal images of D) FAs and (E) YAP/TAZ localization in cells on stiff substrates, treated with different concentrations of AMPK inhibitor (from 0 to 20 µM). Stains: vinculin (green), YAP/TAZ (green), F-actin and nuclei were counterstained with phalloidin (red) and DAPI (blue). Scale bars, 50 µm. (F) Quantification of cell area (n>25 representative cells, N=3) and number of FAs (n>25 representative cells, N=3) and YAP/TAZ nuclear localization (n>40 representative cells, N=3) in single cells on stiff substrate treated with different concentrations of AMPK inhibitor. (G) Expression of G-actin, RhoA, β-integrin and Myosin II (green, from left to right) in cells treated with (bottom) or without (top) AMPK inhibitor. Scale bars, 50 µm. Graph: quantification of Myosin II intensity of the cells (n>20 representative cells from two independent experiments). (H) Cell proliferation on stiff substrates with (bottom) or without (top) AMPK inhibitor as determined by EdU assay. Confocal images show merged intensities of EdU (red) and DAPI (blue). Graph: quantification of EdU positive (proliferating) cells (n>6 representative images, N=3). Scale bars, 200 µm.

2.5 AMPK-mediated ATP production is required for cellular mechanoresponse

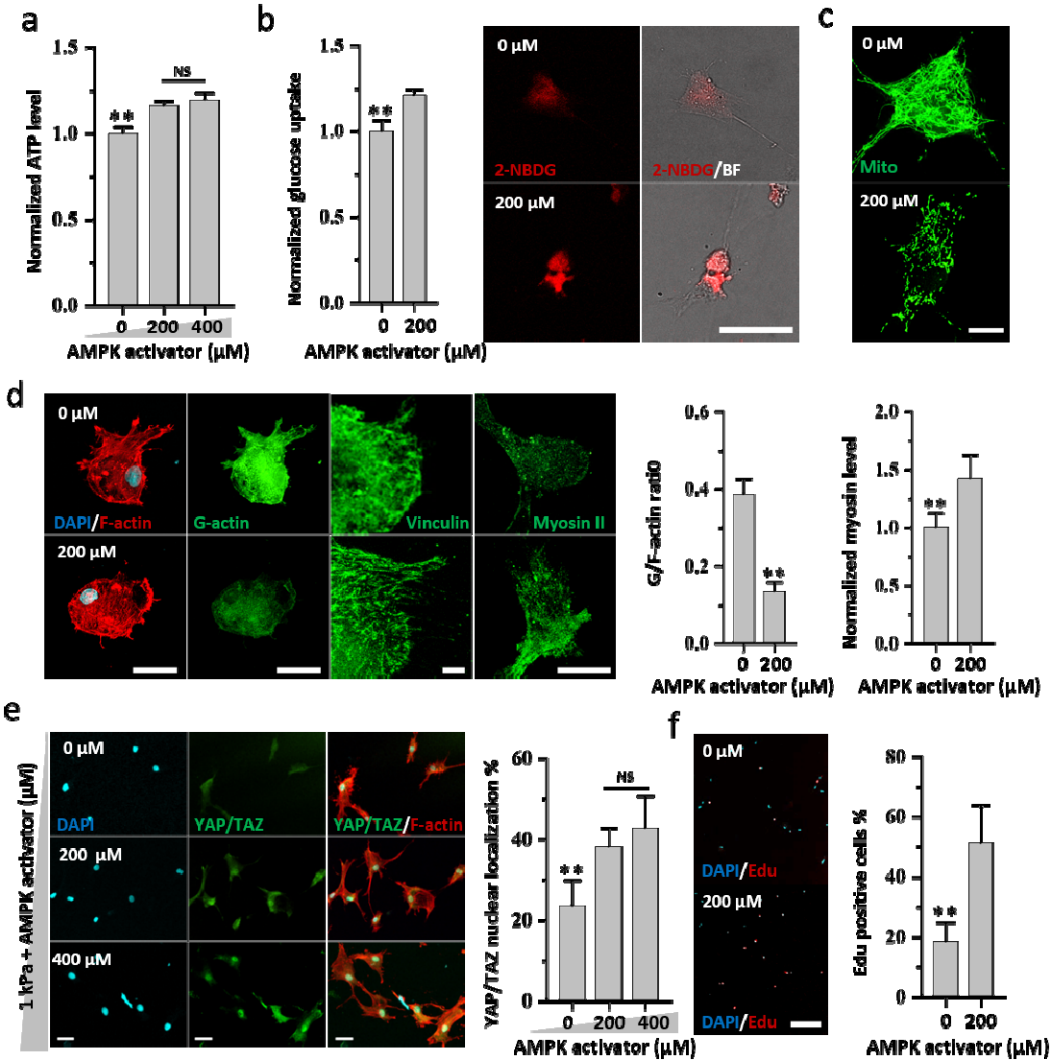

Fig. 5 AMPK activation on soft substrates promotes YAP/TAZ nuclear shuttling. (A) ATP levels in cells on soft substrates treated with AMPK activator (A-769662) (n=5, N=3) after 20 h culture. (B) Comparison of glucose uptake in the presence or absence of AMPK activator. Graph: quantification of glucose uptake (n=5, N=3). Confocal images showing 2-NBDG (red) uptake. Scale bars, 100 µm. (C) Mitochondrial morphologies on soft substrate with (bottom) or without (top) AMPK activator. Scale bars, 10 µm. (D) Expressions of G-actin, vinculin and myosin II

(green, from left to right) in cells with (bottom) or without (top) AMPK activator. Scale bars, 50 µm. Graph: quantification of G/F actin ratio and myosin II intensity (n>20 representative cells from two independent experiments). (E) YAP/TAZ nuclear localization in the presence of different concentrations of AMPK activator. Graph: quantification of YAP/TAZ nuclear localization (n>40 representative cells, N=3). Scale bars, 50 µm. (F) Cell proliferation with (bottom) or without (top) AMPK activator as determined by Edu assay. Confocal images show merged intensities of Edu (red) and DAPI (blue). Graph: quantification of EdU positive (proliferating) cells (n>6 representative images, N=3). Scale bars, 200 µm.

Having demonstrated the effect of AMPK inhibition in cells spreading on stiff substrates, we next studied AMPK activation by adding the AMPK activator, A-769662 after 30 min of cell spreading on soft substrates (using a culture medium containing 4.5 g/L glucose), and culturing cells for 20h. A-769662 treatment increased intracellular ATP levels (up to ~1.9-fold), and increased glucose uptake (up to ~2.3-fold) (**Fig. 5a, b**). Moreover, activation of AMPK triggered a fragmented mitochondrial phenotype (**Fig. 5c**). The increase in ATP levels was paralleled by lower G-actin levels, increased FA formation and enhancement of actomyosin contractility (**Fig. 5d**). We monitored YAP/TAZ localization of hMSCs on soft substrates treated with different concentrations of A-769662. Interestingly, while cells on stiff substrates showed increasing levels of cytoplasmic YAP/TAZ upon inhibition of AMPK, we now observed preferential nuclear YAP/TAZ localization in cells on soft substrates upon AMPK activation (**Fig. 5e**). Compared to the cells on the soft substrate, the additional AMPK activation promoted cellular proliferation 2.6-fold (**Fig. 5f**).

2.6 AMPK activity influences differentiation into osteoblasts

Finally, we determined how manipulation of AMPK activation impacted on cell fate. Runx2 protein is a prominent transcription factor which can be detected in pre-osteoblasts and induces the differentiation of MSCs into osteoblasts when translocated into the nucleus of stem cells [34, 35]. Compound C (10 µM) was added to the medium for cells cultured on stiff substrates and A-769662 (200 µM) was added to the medium for cells on soft substrates. Relative to standard culture conditions, a higher Runx2 nuclear localization was detected under conditions that promote higher AMPK activation on stiff substrates (*i.e.* with no inhibitor present) (**Fig. 6a**) or additional AMPK activator on soft substrates (**Fig. 6b**) after 1-day culture. Further, hMSCs were seeded on stiff and soft substrate and cultured in mixed adipogenic/osteogenic differentiation medium. After 7-10 days culture time, ALP staining was used to indicate osteogenic differentiation and Oil Red O staining was performed for adipogenic differentiation. ALP staining showed AMPK inhibition in cells on stiff substrates significantly decreased ALP

intensity, indicating lower osteogenic differentiation, whereas on soft substrates ALP staining was clearly more intense in the presence of AMPK activator (**Fig. 6a, b**). However, no statistically relevant differences were observed for Oil Red O staining of cells cultured on soft or stiff substrates (and with either AMPK activator or inhibitor, respectively) (**Supplementary Fig. 9**). These results indicate that energy metabolism, as controlled by AMPK, competes with, or overrides, the impact of biophysical cues.

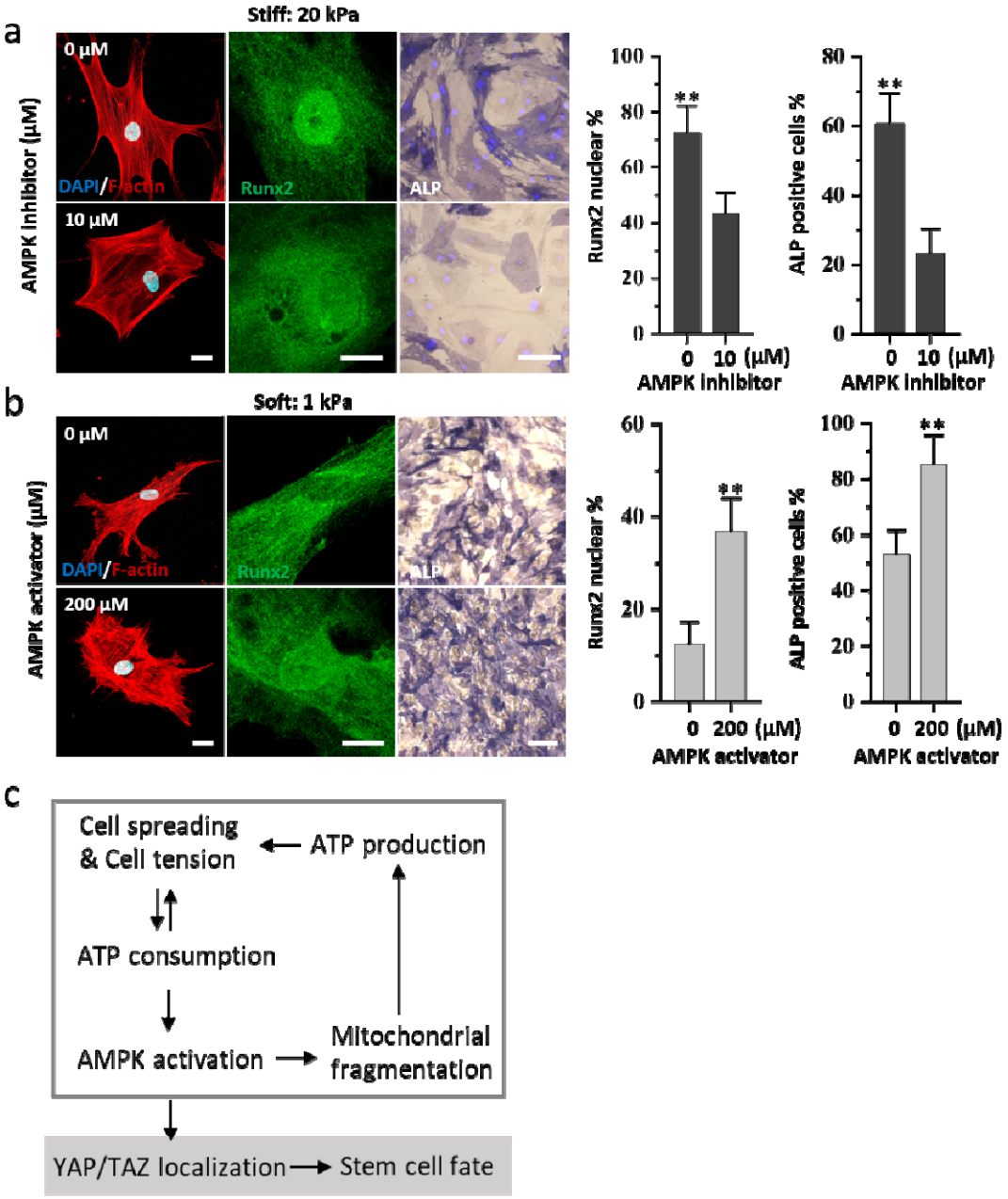

Fig. 6 AMPK inhibition or activation affects stem cell differentiation. (A, B) Runx2 and alkaline phosphatase (ALP) staining showing osteogenic differentiation of hMSCs. Runx2 (green) localization and ALP (bright field) expression of the cells treated with (A) AMPK inhibitor on stiff substrates or (B) AMPK activator on soft substrates (bottom). Scale bars 20 µm (fluorescence images), 250 µm (bright field images). Graph: quantification of Runx2 nuclear localization after 1 day (n>30 representative cell from two independent experiments) and ALP positive cells after 7 days (n>6 representative images from two independent experiments) at different conditions. (C) Schematic overview showing the link between meachnotransduction and energy homeostasis.

3. Discussion

Cells respond to the mechanical properties of the ECM by adjusting the contractility of their actin cytoskeleton, which requires well-developed FAs and well-defined stress fibers [1, 5, 36]. We demonstrate a clear link between mechanotransduction and the energy expenditure needed for the formation of well-developed FAs, cytoskeletal reorganization into well-defined stress fibers in spread cells, as well as the contractility of the cytoskeleton. Intracellular ATP levels are strongly affected by these energetically costly processes. Experiments disrupting cytoskeletal organization or limiting cell contractility reveal that approximately 20% of cellular ATP is consumed by these processes. A further link between energy metabolism and development of the actin cytoskeleton is highlighted by glucose starvation experiments. In the latter, glucose depletion significantly reduces actin polymerization and FAs formation, confirming that cellular mechano-responses consume a significant fraction of intracellular ATP. We demonstrate that cell spreading on stiff substrates is associated with an initial drop in ATP levels. This drop activates AMPK, a kinase that is triggered by changing AMP/ATP ratios that arise from, for example, starvation, hypoxia or cell detachment from the matrix [18, 19]. AMPK plays a central role in the coordination of cell metabolism and function [17]. We here provide evidence that AMPK effectuates increased cellular glucose uptake, mitochondrial fragmentation and nuclear localization of YAP/TAZ. Experiments with AMPKα-null cells firmly established the central role of AMPK in translating the initial spreading response on stiff substrates into elevated ATP levels at steady state. We further observed that osteogenic differentiation appears correlated with activation of inhibition of AMPK, and not with the substrate stiffness. In summary, our findings provide a long-elusive mechanism for the mechanoresponse of cell via the activation of AMPK. This response is initiated by cell spreading and the concomitant consumption of ATP (**Fig. 6c**), which leads to further spreading and increased cell tension as the actin cytoskeleton organizes and FAs form. ATP expenditure exceeds production, thus leading to a drop in ATP levels and activation of AMPK. AMPK then activates energy metabolism and mitochondrial

morphodynamics, while at the same time influencing YAP/TAZ localization and, ultimately, osteogenic differentiation.

Taken together, this work establishes temporal changes in intracellular ATP levels during cell spreading as a new mechanistic link between mechanical forces and molecular responses. In this sense, energy expenditure couples mechanical cues with cellular metabolism via AMPK activation in response to lowered ATP levels. These findings provide an impetus for further studies into the mechanisms that guide energy metabolic remodeling in cells with increased energy demands during their response to environmental cues. Of particular interest in this context is how the remodeled energy metabolism in tumor cells shapes their mechanoresponse to ECM alterations.

Acknowledgments

We thank José M. A. Hendriks for assistance with cell cultures, and Dr. Liesbeth Pierson for assistance with confocal microscopy. We thank Dr. Benoit Viollet (Paris Descartes University) for providing WT-MEF and AMPKα-null MEF cell lines. J.X., M.B. and X.H. would like acknowledge the department of General Instruments of the Radboud University for providing confocal and light microscopy services. We acknowledge financial support from the China Scholarship Council (J.X. and X.H.) and the Radboud Nanomedicine Alliance (M.B.).

Author contributions

J.X. and M.B. contributed equally to this work. W.T.S.H. supervised the research. J.X., M.B. and W.T.S.H. planned the project and designed all experiments. J.X. and M.B. carried out all the experiments and performed image analyses. W.J.H.K. performed the mitochondrial morphology quantifications. X.H. provided assistance with western blots and cell culture. All authors contributed to writing the manuscript.

Conflict of interest

W.J.H.K. is a scientific advisor of Khondrion B.V. (Nijmegen, The Netherlands) and Fortify Therapeutics (Palo Alto, USA). These SMEs had no involvement in the data collection, analysis and interpretation, writing of the manuscript, and in the decision to submit the manuscript for publication.

References

1. Discher, D.E., Janmey, P. & Wang, Y.L. Tissue cells feel and respond to the stiffness of their substrate. *Science* **310**, 1139-1143 (2005).
2. Engler, A.J., Shamik, S., H Lee, S. & Discher, D.E. Matrix elasticity directs stem cell lineage specification. *Cell* **126**, 677-689 (2006).
3. Elosegui-Artola, A. *et al.* Force Triggers YAP Nuclear Entry by Regulating Transport across Nuclear Pores. *Cell* **171**, 1397-1410 (2017).
4. Trappmann, B. *et al.* Extracellular-matrix tethering regulates stem-cell fate. *Nat. Mater.* **11**, 642 (2012).
5. Yeung, T. *et al.* Effects of substrate stiffness on cell morphology, cytoskeletal structure, and adhesion. *Cell Motil. Cytoskel.* **60**, 24-34 (2005).
6. Vogel, V. & Sheetz, M. Local force and geometry sensing regulate cell functions. *Nat. Rev. Mol. Cell Biol.* **7**, 265 (2006).
7. Choquet, D., Felsenfeld, D.P. & Sheetz, M.P. Extracellular matrix rigidity causes strengthening of integrin-cytoskeleton linkages. *Cell* **88**, 39-48 (1997).
8. Adams, J. Cell-matrix contact structures. *Cell. Mol. Life Sci.* **58**, 371-392 (2001).
9. Chen, C.S., Tan, J. & Tien, J. Mechanotransduction at cell-matrix and cell-cell contacts. *Annu. Rev. Biomed. Eng.* **6**, 275-302 (2004).
10. Mih, J.D., Marinkovic, A., Liu, F., Sharif, A.S. & Tschumperlin, D.J. Matrix stiffness reverses the effect of actomyosin tension on cell proliferation. *J. Cell Sci.* **125**, 5974-5983 (2012).
11. Bays, J.L., Campbell, H.K., Heidema, C., Sebbagh, M. & DeMali, K.A. Linking E-cadherin mechanotransduction to cell metabolism through force-mediated activation of AMPK. *Nat. Cell Biol.* **19**, 724-731 (2017).
12. Salvi, A.M. & DeMali, K.A. Mechanisms linking mechanotransduction and cell metabolism. *Curr. Opin. Cell Biol.* **54**, 114-120 (2018).
13. Romani, P. *et al.* Extracellular matrix mechanical cues regulate lipid metabolism through Lipin-1 and SREBP. *Nat. Cell Biol.*, 338-347 (2019).
14. Bartoláksuki, E. *et al.* Fluctuation-driven mechanotransduction regulates mitochondrial-network structure and function. *Nat. Mater.* **14**, 1049-1057 (2015).
15. Gowans, G.J. & Hardie, D.G. AMPK: a cellular energy sensor primarily regulated by AMP. *Biochem. Soc. Trans.* **42**, 71-75 (2014).
16. Zhao, H. *et al.* AMPK-mediated activation of MCU stimulates mitochondrial Ca(2+) entry to promote mitotic progression. *Nat. Cell Biol.*, 476-486 (2019).
17. Kahn, B.B., Thierry, A., David, C. & Hardie, D.G. AMP-activated protein kinase: ancient energy gauge provides clues to modern understanding of metabolism. *Cell Metabol.* **1**, 15-25 (2005).
18. Hardie, D.G., D. Carling & Carlson, M. The AMP-activated/SNF1 protein kinase subfamily: metabolic sensors of the eukaryotic cell. *Annu. Rev. Biochem.* **67**, 821-855 (1998).
19. Jung-Soon, M. *et al.* Cellular energy stress induces AMPK-mediated regulation of YAP and the Hippo pathway. *Nat. Cell Biol.* **17**, 500-510 (2015).
20. Hardie, D.G., Ross, F.A. & Hawley, S.A. AMPK: a nutrient and energy sensor that maintains energy homeostasis. *Nat. Rev. Mol. Cell Biol.* **13**, 251 (2012).

21. Herzig, S. & Shaw, R.J. AMPK: guardian of metabolism and mitochondrial homeostasis. *Nat. Rev. Mol. Cell Biol.* **19**, 121-135 (2018).
22. Toyama, E.Q. *et al.* AMP-activated protein kinase mediates mitochondrial fission in response to energy stress. *Science* **351**, 275-281 (2016).
23. Helle, S.C.J. *et al.* Mechanical force induces mitochondrial fission. *Elife* **6**, e30292 (2017).
24. Rambold, A.S., Kostelecky, B., Elia, N. & Lippincott-Schwartz, J. Tubular network formation protects mitochondria from autophagosomal degradation during nutrient starvation. *Proc. Natl. Acad. Sci.* **108**, 10190-10195 (2011).
25. Inoki, K., Zhu, T. & Guan, K.L. TSC2 Mediates Cellular Energy Response to Control Cell Growth and Survival. *Cell* **115**, 577-590 (2003).
26. Bernstein, B.W. & Bamburg, J.R. Actin-ATP Hydrolysis Is a Major Energy Drain for Neurons. *J. Neurosci.* **23**, 1-6 (2003).
27. Khacho, M. *et al.* Mitochondrial Dynamics Impacts Stem Cell Identity and Fate Decisions by Regulating a Nuclear Transcriptional Program. *Cell Stem Cell* **19**, 232-247 (2016).
28. Koopman, W.J., Distelmaier, F., Esseling, J.J., Smeitink, J.A. & Willems, P.H. Computer-assisted live cell analysis of mitochondrial membrane potential, morphology and calcium handling. *Methods* **46**, 304-311 (2008).
29. Sirio, D. *et al.* Role of YAP/TAZ in mechanotransduction. *Nature* **474**, 179-183 (2011).
30. Meng, Z. *et al.* RAP2 mediates mechanoresponses of the Hippo pathway. *Nature* **560**, 655-660 (2018).
31. Valon, L., Marín-Llauradó, A., Wyatt, T., Charras, G. & Trepat, X. Optogenetic control of cellular forces and mechanotransduction. *Nat. Comm.* **8**, 14396 (2017).
32. Mcbeath, R., Pirone, D.M., Nelson, C.M., Bhadriraju, K. & Chen, C.S. Cell Shape, Cytoskeletal Tension, and RhoA Regulate Stem Cell Lineage Commitment. *Dev. Cell* **6**, 483-495 (2004).
33. Schiller, H.B. *et al.* β1- and αv-class integrins cooperate to regulate myosin II during rigidity sensing of fibronectin-based microenvironments. *Nat. Cell Biol.* **15**, 625-636 (2013).
34. Chun, Y., Tibbitt, M.W., Lena, B. & Anseth, K.S. Mechanical memory and dosing influence stem cell fate. *Nat. Mater.* **13**, 645-652 (2014).
35. Zhuoran, Z., Ming, Z., Guozhi, X. & Franceschi, R.T. Gene transfer of the Runx2 transcription factor enhances osteogenic activity of bone marrow stromal cells in vitro and in vivo. *Mol. Ther.* **12**, 247-253 (2005).
36. Bao, M., Xie, J., Piruska, A. & Huck, W.T. 3D microniches reveal the importance of cell size and shape. *Nat. Comm.* **8**, 1962 (2017).